INTERNATIONAL JOURNAL FOR NUMERICAL METHODS IN FLUIDS, VOL. 14, 1347–1365 (1992)

BOUNDARY ELEMENT METHOD FOR LONG-TIME WATER WAVE PROPAGATION OVER RAPIDLY VARYING BOTTOM TOPOGRAPHY

A. NACHBIN* AND G. C. PAPANICOLAOU

Courant Institute of Mathematical Sciences, New York University, 251 Mercer Street, New York, NY 10012, U.S.A.

SUMMARY

We study numerically the linear water wave equations for shallow channels with rapidly varying bottom topography. We do not use the shallow water approximation because it is not valid when the bottom is rapidly varying. We use the boundary element method because it allows accurate tracking of the surface waves for long times. We present the results of a range of numerical validation experiments and a comparison between propagation over a periodic and a random rough bottom topography.

KEY WORDS Water waves Wave reflection and transmission Boundary element method Asymptotic theory

1. INTRODUCTION

Our primary interest is in studying the propagation of linear water waves in shallow channels in the presence of a rapidly varying random bottom topography. We have developed an analytical theory for wave reflection based on the asymptotic analysis of stochastic differential equations.[1] We use the full water wave equations and not the shallow water approximation which is not valid[2] in channels with a rapidly varying bottom. In this paper we use the boundary element method to compute numerically surface waves propagating over rapidly varying bottom topographies. We perform several numerical experiments which show that the numerical method gives very good results in the regime of the asymptotic theory.

Let $\phi(x, y, t)$ be the velocity potential and $\eta(x, t)$ the surface elevation. The scaled and dimensionless linear water wave equations are

$$\beta^2 \phi_{xx} + \phi_{yy} = 0 \tag{1}$$

for interior points of the fluid body, with the free surface conditions

$$\left.\begin{aligned} \eta_t - (1/\beta^2)\phi_y = 0 \\ \eta + \phi_t = 0 \end{aligned}\right\} \quad \text{on } y = 0 \tag{2}$$

and a Neumann condition at the bottom,

$$\phi_y + \beta^2 h'(x)\phi_x = 0 \quad \text{on} \quad y = -h(x) = -1 + H(x), \qquad |H(x)| < 1. \tag{3}$$

---

*Present address: Department of Mathematics, The Ohio State University, 231 W 18th Avenue, Columbus, OH 43210-1174, U.S.A.

0271–2091/92/111347–19$09.50

Received 16 August 1990
Revised 21 October 1991

The bottom topography is given by $y=-1+H(x)$ and the initial data are $\phi(x, 0, 0)$ and $\phi_t(x, 0, 0)=-\eta(x, 0)$. We are interested in cases where $\eta(x, 0)$ has the form of a pulse. The scaling is the same as in References 3 and 4. The parameter β is the ratio of a characteristic depth and a characteristic wavelength. When β is small, the channel is shallow.

Surface water wave propagation is dispersive so the numerical method must accurately reproduce the dispersive effects in the solution. We tested two methods: the finite difference method (FDM) and the boundary element method (BEM). We computed the exact solution to the difference equations (time harmonic FDM) for an arbitrary mesh. We studied different approximations for the y-derivative (in the free surface condition) and its corresponding numerical dispersion relations. We carried out several numerical experiments. We observed that the optimal mesh ratio $\Delta x/\Delta t$ is related to the phase speed, which depends on the wave number. Thus the difference scheme developed is a restrictive method for problems involving a full band of frequencies. We present the analysis and the corresponding results in the Appendix.

We find that when suitably implemented, the boundary element method has very good dispersive properties over a broad range of frequencies. We have done several numerical experiments to test the performance of this method. First we have compared numerical computations of wave pulses propagating over a flat bottom with the near-wavefront approximation of the exact solution and found very good agreement. Then we compared the numerical solutions of wave pulses propagating over a rapidly varying periodic bottom with the results of the asymptotic theory given in Reference 4. This theory predicts that long waves propagate as if in an effective channel with a flat bottom and with a speed slightly smaller than the one for the flat channel. We find very good agreement between theoretical and computational results. We note that this is a severe test of the performance of the numerical method.

Finally we have computed numerically the reflection of waves in a channel with a random bottom topography. As expected,[1] there is a great deal of difference between propagation over a periodic and a random bottom because of wave localization in the random case. The boundary element method is thus well suited for capturing different effects in wave propagation in channels with periodic and random bottoms.

2. THE BOUNDARY ELEMENT METHOD

2.1. Description of the method

We will review briefly the boundary element method,[5] indicating some small modifications that are needed in the implementation. Let Ω be the flow domain with the boundary $\partial\Omega$ divided into four parts:

Γ_1 and Γ_4 → the left and right ends of the channel
Γ_2 → the linear free surface
Γ_3 → the impermeable bottom (not necessarily flat).

The potential $\phi(x, y, t)=\phi(P, t)$ satisfies the integral equation

$$\beta\theta_P\phi(P, t)=\oint_{\partial\Omega}\left(\phi(Q, t)\frac{\mathrm{d}(\ln\rho)}{\mathrm{d}\bar{n}}-\phi_{\bar{n}}(Q, t)\ln\rho\right)\mathrm{d}Q, \tag{4}$$

where

$$\theta_P=\begin{cases}\pi & \text{if } P \text{ is at a smooth part of } \partial\Omega,\\ \text{internal angle} & \text{if } P \text{ is at a corner of } \partial\Omega,\end{cases} \tag{5}$$

with the free surface conditions

$$\left.\begin{aligned}\phi_t &= -\eta \\ \eta_t &= (1/\beta^2)\phi_y\end{aligned}\right\} \quad \text{at } \Gamma_2, \tag{6}$$

the bottom condition

$$\phi_{\bar{n}} = 0 \quad \text{at } \Gamma_3 \tag{7}$$

and the approximate radiation condition

$$(1/\beta^2)\phi_{\bar{n}} = -\phi_t \quad \text{at } \Gamma_1 \text{ and } \Gamma_4. \tag{8}$$

We use the notation $\mathrm{d}/\mathrm{d}\bar{n} = (\beta^2\partial/\partial_x, \partial/\partial_y)\cdot(n_1, n_2)$, where $\vec{n}$ is the outward normal vector to $\partial\Omega$, $\rho = \sqrt{[(x_p - x_q)^2 + \beta^2(y_p - y_q)^2]}$ and $\mathrm{d}Q$ is a line element. The radiation condition allows waves with unit speed (i.e. the dimensionless shallow water speed) to propagate out of the computational domain. Owing to dispersion and the nature of the pulse-shaped waves, equation (8) is an approximate radiation condition. For shallow channels (i.e. β small) the dominant modes in our experiments are such that $k\beta$ is small and therefore their phase speed is close to the dimensionless shallow water speed.

We use the point collocation method and linear elements to discretize the integral equation.[6] We derive exact integration formulae, similar to the ones presented by Nakayama and Washizu,[7] with the difference that the depth effect is retained through the parameter β. With these formulae we calculate efficiently (through vectorization) the influence of the source points and dipoles, located at the end nodes of a given boundary element, on all field points P_i of our mesh. We would normally integrate over the contour $\partial\Omega$, but the pattern of the analytic integration formulae[7,8] naturally suggests inverting this procedure. Consequently, vectorization is a straightforward task.

We use the same differencing schemes for the boundary conditions as those in Reference 5 but with the parameter β introduced. An implicit free surface condition is derived by combining finite difference approximations to the Bernoulli law and the kinematic condition, both at time $t = (n+\frac{1}{2})\Delta t$. This leads to

$$\frac{\phi^{n+1} - \phi^n}{\Delta t} = -\left(\eta^n + \frac{\Delta t}{2\beta^2}(\theta\phi_y^{n+1} + (1-\theta)\phi_y^n)\right) + O(\Delta t^2), \tag{9}$$

which is used in the discrete integral equation. To update the water elevation $\eta(x, t)$, we use the discrete kinematic condition at time $t = (n+\frac{1}{2})\Delta t$,

$$\frac{\eta^{n+1} - \eta^n}{\Delta t} = \frac{\phi_y^{n+1} + \phi_y^n}{2\beta^2} + O(\Delta t^2). \tag{10}$$

The parameter θ is the implicit time-weighting factor. In the next subsection we present a truncation error analysis through which we find its optimal value to be $\theta = \frac{1}{6}$. We also use the discrete radiation condition

$$\frac{\phi_{\bar{n}}^{n+1}}{\beta^2} = \frac{\phi^{n+1} - \phi^n}{\Delta t}.$$

We need to take special care at the corner nodes of the free surface. Three unknowns are associated with each of these nodes: ϕ and the normal derivatives (to each side) ϕ_x and ϕ_y. We want to solve for ϕ_y. In order to eliminate the other two parameters, we proceed as follows. For the vertical boundary element (containing the corner node) we use the radiation condition to substitute the normal derivative in the integral equation by the actual value of the potential. The

potential is continuous and we use the free surface condition to substitute it for its y-derivative. Thus we have one unknown at the corner nodes for both the vertical and horizontal elements sharing this node.

We define the vector of unknowns by

$$[\phi_{\Gamma_1}^{n+1}/\Delta t \quad \cdots \quad \phi_{y\Gamma_2}^{n+1}/\beta^2 \quad \cdots \quad \phi_{\Gamma_3}^{n+1} \quad \cdots \quad \phi_{\Gamma_4}^{n+1}/\Delta t].$$

We partitioned this vector according to the type of boundary indicated in the subscript. We also scaled the unknowns so that all entries of the matrices are of the same order and consequently the system is better conditioned.

2.2. *Dispersion analysis for the free surface evolution scheme*

We will suppose that the integral equation has been solved exactly at some time t. We then analyse the dispersive properties of the evolution scheme along the free surface. We eliminate η from the difference scheme (equations (9) and (10)) and get

$$D_\theta\phi \equiv \frac{\phi^{n+1}-2\phi^n+\phi^{n-1}}{\Delta t^2}+\frac{1}{2\beta^2}[\theta\phi_y^{n+1}+2(1-\theta)\phi_y^n+\theta\phi_y^{n-1}]=0. \tag{11}$$

The parameter $\theta\in[0, 1]$ defines how we average the normal components ϕ_y of the velocity. We will show how to determine it for best results.

First we present a concise description of the dispersion analysis given by Salmon *et al.*[5] In order to derive an expression for the relative error of the frequency, they substitute the Fourier mode $\phi(x, y, t)=\cosh[k\beta(1+y)]\exp[\mathrm{i}(kx-\omega t)]$ in the equation above and write the numerical dispersion relation for the time evolution difference scheme. It is given in the form of a quadratic equation,

$$(1+\theta p)\mathrm{e}^{-2\mathrm{i}\omega\Delta t}-2[1-(1-\theta)p]\mathrm{e}^{-\mathrm{i}\omega\Delta t}+1+\theta p=0, \tag{12}$$

where

$$p\equiv\Delta t^2\frac{k\tanh(k\beta)}{2\beta}. \tag{13}$$

The root related to the correct right-going mode is

$$\mathrm{e}^{-\mathrm{i}\omega\Delta t}=\frac{2[1-p(1-\theta)]-\mathrm{i}\sqrt{[8p-4p^2(1-2\theta)]}}{2(1+p\theta)}=a-\mathrm{i}b.$$

We must have $a^2+b^2=1$ for no dissipation/amplification. We can readily check that this is true. In the expression above there is a hidden stability condition: the discriminant of the quadratic equation must be negative so that the roots are conjugate complex numbers.

The root's argument will lead to an expression for the numerical frequency,

$$\omega\Delta t=\tan^{-1}\left(\frac{b}{a}\right)=\tan^{-1}\left(\frac{\sqrt{[2p-p^2(1-2\theta)]}}{1-p(1-\theta)}\right).$$

When we refer back to the definition of p, we see that

$$\sqrt{(2p)}=\omega_{\text{exact}}\Delta t\equiv z.$$

The exact frequency ω_{exact} is obtained from the dispersion relation

$$\omega^2=\frac{k}{\beta}\tanh(k\beta). \tag{14}$$

The relative error for the frequency is given by

$$\frac{\omega-\omega_{\text{exact}}}{\omega}=\left[\tan^{-1}\left(\frac{2z\sqrt{[1-z^2(1-2\theta)/4]}}{2-z^2(1-\theta)}\right)-z\right]z^{-1}. \tag{15}$$

Salmon *et al.* plotted curves which show the dependence of this error on the parameter θ. We have reproduced some of these curves in Figure 1. They suggest the value $\theta=0{\cdot}17$, but for small Δt we see that the value $\theta=0{\cdot}165$ leads to a better approximation. This family of curves is interesting because we can see that a full band of frequencies can be approximated well. This is an important feature for problems involving pulse-shaped waves.

We now present a different dispersion analysis which will lead to the optimal value of the parameter θ. We write the numerical dispersion relation as

$$\cos(\omega\Delta t)=\frac{2-(1-\theta)z^2}{2+\theta z^2}\equiv\psi(z).$$

In Reference 5 the condition for stability is that the roots defined above are such that $a^2+b^2=1$. No explicit constraint for Δt is given. The true condition for stability can be found in their analytical calculations. We see from the numerical dispersion relation given above that unconditional stability implies $|\psi(z)|\leqslant 1$ and therefore $\theta\geqslant\frac{1}{2}$. We know that our scheme is only conditionally stable since $\theta\approx 0{\cdot}17$. This gives a constraint on the time step.

We now show how to find the best value of θ. We take equation (11) and consider the Taylor expansions that generated this scheme. We obtain the one-parameter family of differential operators (for small time steps)

$$D_\theta\phi=\phi_{tt}+\frac{1}{\beta^2}\phi_y+\frac{\Delta t^2}{12}\left(\phi_{ttt}+\frac{6\theta}{\beta^2}\phi_{ytt}\right)+\frac{\Delta t^4}{360}\left(\phi_{tttttt}+\frac{30\theta}{\beta^2}\phi_{ytttt}\right)+\cdots=0. \tag{16}$$

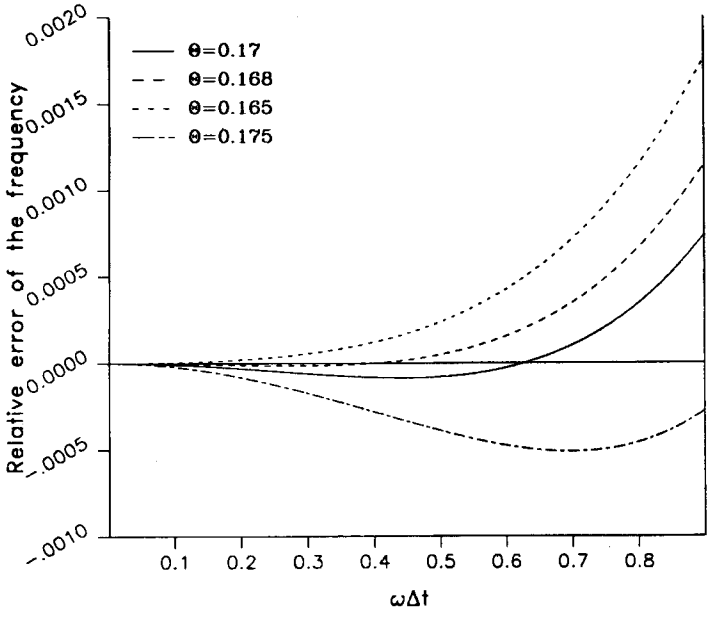

Figure 1. Numerical frequencies' error for different values of θ

We suppose that the time step is small enough so that the fourth-order differential equation obtained from the first four terms is considered as a continuum version of the difference scheme. Its properties are more closely related to the difference scheme than those of the original equation (obtained when $\Delta t = 0$). If we let $\theta = \frac{1}{6} = 0{\cdot}1666\ldots$, this equation has the *same* dispersion relation as our original problem. Hence $\theta = 0{\cdot}17$ is a very good approximation for this parameter but its optimal value is $\frac{1}{6}$. In other words, D_θ will be a fourth-order scheme if we take this value. The stability condition for the scheme with $\theta = \frac{1}{6}$ is

$$\Delta t \leqslant \frac{\sqrt{6}}{\omega}.$$

3. NUMERICAL ASYMPTOTICS USING THE BOUNDARY ELEMENT METHOD

3.1. Gaussian pulse propagating over a flat bottom

We are dealing with a boundary–initial value problem. Given the initial data for the water elevation we need to compute the initial boundary data (Dirichlet and Neumann) for the wave potential ϕ. In the asymptotic theory presented in Reference 1 the initial disturbance is assumed to be propagating (at time $t = 0$) with unit speed. It is an exact solution only in the $\beta = 0$ limit. In the present study we consider approximate initial data for the potential. We observed the numerical consequences of this approximation and found that the error made is negligible.

We want to study computationally the propagation of a wave with the initial elevation given by

$$\eta(x, 0) = e^{-x^2/\sigma^2}, \qquad \eta_t(x, 0) = \frac{2x}{\sigma^2} e^{-x^2/\sigma^2}.$$

We now calculate the approximate Dirichlet and Neumann data for the potential. We consider that at time $t = 0$, η and ϕ are functions of $x - t$ (as in Reference 1). We write for the initial velocity potential (using the linear Bernoulli law) that

$$\phi(x, 0, 0) = \sigma \int_{-\infty}^{x/\sigma} e^{-u^2}\, du.$$

We calculate the initial Neumann condition from the kinematic condition to get

$$\phi_y(x, 0, 0) = \beta^2 \eta_t(x, 0) = \frac{2\beta^2}{\sigma^2} x e^{-x^2/\sigma^2}.$$

The approximate initial Dirichlet and Neumann conditions at the free surface are

$$\phi^0 = 0{\cdot}5\sigma\sqrt{\pi}\left[1 + \operatorname{erf}\left(\frac{x}{\sigma}\right)\right], \qquad \frac{\phi_y^0}{\beta^2} = \frac{2x}{\sigma^2} e^{-x^2/\sigma^2},$$

where $\operatorname{erf}(x)$ is the error function.[9] We find the order of the approximation made by looking at the Fourier transform of the initial conditions. We compare it with the exact ones to see that the error made in the Fourier coefficients of the initial Dirichlet and Neumann data is $O(k^2\beta^2)$. This error is negligible along the wavefront where small wave numbers k are dominant. We will confirm this fact numerically.

We have the complete set of (approximate) boundary data along Γ_2. The normal derivative at the bottom Γ_3 is always zero and we do not need to know the initial potential along the bottom. We compute the initial value of the potential along the lateral boundaries Γ_1 and Γ_4, by extending

its value at the corners of the free surface all the way to the bottom. This is again an approximation taking into account that $\beta \ll 1$ and that the ends of the channel are far enough from the centre of the Gaussian pulse.

We will compare the long-time behaviour of the computed solution with a near-wavefront approximation of the Fourier representation of the exact solution. We have a full band of frequencies and therefore this is an important test for the BEM's dispersive behaviour.

Let the parameter β be small so that we are in the finite depth, shallow water regime. We still have a dispersive system although the depth is small compared to the wavelength. We let $\omega = \pm W(k)$ be the two modes obtained from the dispersion relation (14). We express the water elevation as a superposition of the right- and left-going modes,

$$\eta(x, t) = \int_{-\infty}^{\infty} F_1(k) e^{i[kx - W(k)t]} dk + \int_{-\infty}^{\infty} F_2(k) e^{i[kx + W(k)t]} dk. \tag{17}$$

We proceed by doing a near-wavefront analysis as in Reference 3. We consider the group moving to the right with unit speed. From a stationary phase analysis we know that the only contribution will come from the stationary points. For the unit group speed we have only $k=0$, where $W''(0)=0$ and $W'''(0)\neq 0$. This indicates an $O(t^{-1/3})$ decay of the front as $t \to \infty$. We expand both the amplitude $F_1(k)$ and the frequency $W(k)$ about $k=0$ for the right-going modes:

$$W(k) \approx k - \frac{\beta^2}{6} k^3, \qquad F_1(k) \approx F_1(0) = \frac{1}{\sqrt{(2\pi)}} \hat{\eta}_0(0) = \frac{\sigma}{2\sqrt{\pi}}.$$

We have taken only the first term in order to be consistent with the stationary phase results. We define $\gamma \equiv \beta^2/6$ and get that

$$\eta(x, t) \sim \frac{\sigma}{2\sqrt{\pi}} (3\gamma t)^{-1/3} \int_{-\infty}^{\infty} \exp\left(izs + i\frac{s^3}{3} \right) ds = \frac{\sigma}{\sqrt{\pi}(3\gamma t)^{1/3}} Ai(z), \tag{18}$$

with $z = (x-t)/(3\gamma t)^{1/3}$ and where $Ai(z)$ is the Airy function.

In our computations we consider $\sigma = 0{\cdot}3$ so that the effective support of the pulse is approximately unity. The effective wave numbers range from zero to 12 (approximately). Using the dispersion relation (with $\beta = 0{\cdot}2$), we have that the effective band of frequencies is in the interval $[0, 8]$.

We let the wave propagate in a long channel 60 times the effective pulse width. We present the results for the long-time behaviour in Figures 2 and 3. The numerical solution agrees with the Airy function in the neighbourhood of the front. Behind the front high-frequency terms dominate and therefore the expansions about $k=0$ are not accurate. There the Airy function is not a good approximation. When we observe the numerical solution at later times (Figure 3) and therefore at a point further away from the origin (note that the shallow water speed is unity), we find that the results agree more closely with the Airy function also in the tail. This shows that the numerical method performs well also for the non-dominant terms when we allow the numerical solution to evolve for long-time intervals.

We verify computationally that our numerical method is stable and conserves the total energy by keeping track of certain conserved quantities. Stoker[11] shows that for linear water waves the total energy

$$E(t) = \frac{\rho}{2} \int_{\Omega} (\nabla \phi)^2 d\Omega + \int_{\Gamma_2} g(\eta^2 - h^2) dx$$

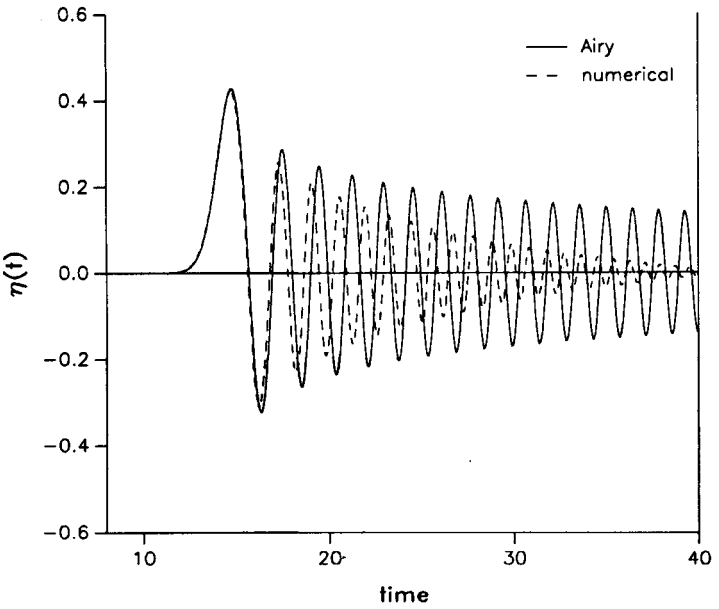

Figure 2. Near-wavefront approximation and numerical solution observed at $x = 14{\cdot}091$ (i.e. Airy function is centred at x) with $\beta = 0{\cdot}2$

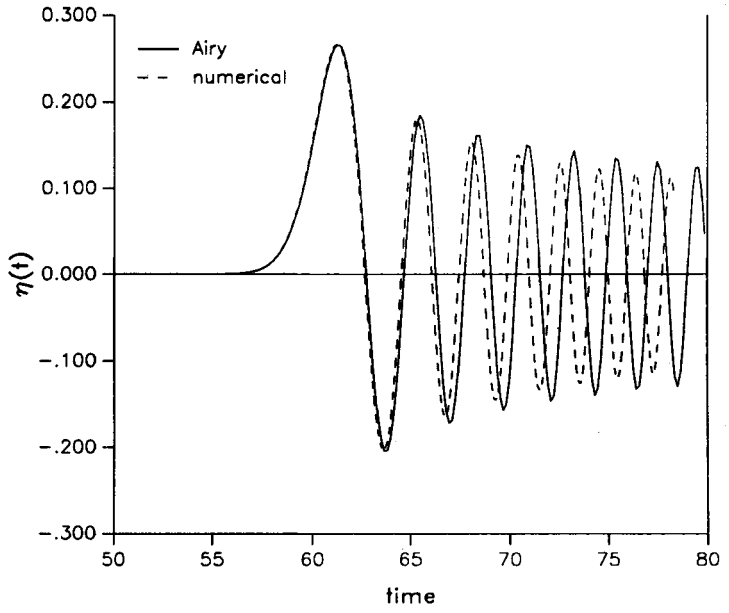

Figure 3. Near-wavefront approximation and numerical solution observed at $x = 60{\cdot}197$ (i.e. Airy function is centred at x) with $\beta = 0{\cdot}2$

is conserved in time. Our code will control two quantities related to the total energy. First we consider the kinetic energy

$$\mathrm{Kin}(t)=\frac{1}{2\beta^2}\int_\Omega (\nabla_\beta \phi)^2 \,\mathrm{d}\Omega,$$

with the gradient defined as $\nabla_\beta=(\beta\partial/\partial_x, \partial/\partial_y)$. We integrate by parts to get

$$\mathrm{Kin}(t)=\frac{1}{2}\oint_{\partial\Omega} \phi\frac{\phi_{\bar{n}}}{\beta^2}\mathrm{d}Q.$$

Next we define as the volume excess the total amount of water added to a previously undisturbed configuration, namely we have that

$$\mathrm{Vol}(t)=\int_{-\infty}^{\infty}\eta(x,t)\,\mathrm{d}x.$$

In order to compute Kin(0) for the problem with a Gaussian pulse, we may consider initially the normal derivative of the potential to be zero at $\Gamma_1\cup\Gamma_3\cup\Gamma_4$ so that integration is restricted to Γ_2:

$$\mathrm{Kin}(0)=-\frac{1}{2}\int_{-\infty}^{\infty}\frac{2}{\sigma^2}x\,\mathrm{e}^{-x^2/\sigma^2}\left(\sigma\int_{-\infty}^{x/\sigma}\mathrm{e}^{-u^2}\,\mathrm{d}u\right)\mathrm{d}x=\frac{\sigma\sqrt{(2\pi)}}{4}.$$

The volume excess will be

$$\mathrm{Vol}(0)=\int_{-\infty}^{\infty}\mathrm{e}^{-x^2/\sigma^2}\,\mathrm{d}x=\sigma\sqrt{\pi}\left(\frac{1}{\sqrt{(2\pi)}}\int_{-\infty}^{\infty}\mathrm{e}^{-u^2/2}\,\mathrm{d}u\right)=\sigma\sqrt{\pi}.$$

We take $\sigma=0{\cdot}3$. Therefore $\mathrm{Kin}(0)=0{\cdot}187\,9971$ and $\mathrm{Vol}(0)=0{\cdot}531\,7362$.

We use Simpson's rule to compute these quantities at each time step. We show how these integrals depend on β in Figures 4 and 5. We can see that as we go into the shallow water regime, the code responds adequately and a more coherent behaviour of the pulse is observed. The limiting features of pure advection are captured for small β.

The oscillations in the volume excess graph show that after the wavefront leaves the computational domain, an oscillatory wavetrain follows (owing to dispersion). These oscillations tend to disappear as β decreases. The oscillations in the kinetic energy (Figure 5) indicate the presence of a velocity component which is not present in the shallow water limit.

We have shown that important quantities are conserved and also that the radiation condition is absorbing the outgoing waves properly.

3.2. Gaussian pulse propagating over a rapidly varying periodic bottom

In Reference 4, Rosales and Papanicolaou show that for the non-linear equations, if we specialize a multiscale asymptotic expansion to right-going disturbances (i.e. using functions of the type $\phi_i(\varepsilon t, x-Ct, x/\sqrt{\varepsilon}, y)$), the effective shallow water speed C can be calculated from a solvability condition. Straightforward inspection of their calculations shows that the same condition is true in the linear case. We assume that the periodic bottom topography is described by the function $y=-h(x)=-1+H(x/\sqrt{\varepsilon})$, with $|H(x/\sqrt{\varepsilon})|<1$ and $H(x/\sqrt{\varepsilon})=H(1+x/\sqrt{\varepsilon})$. The solvability condition for the second term in the expansion (i.e. the order-$\sqrt{\varepsilon}$ equations) leads to the formula

$$C^2=1-\int_0^1 h_z(z)A(z,-h(z))\,\mathrm{d}z<1. \tag{19}$$

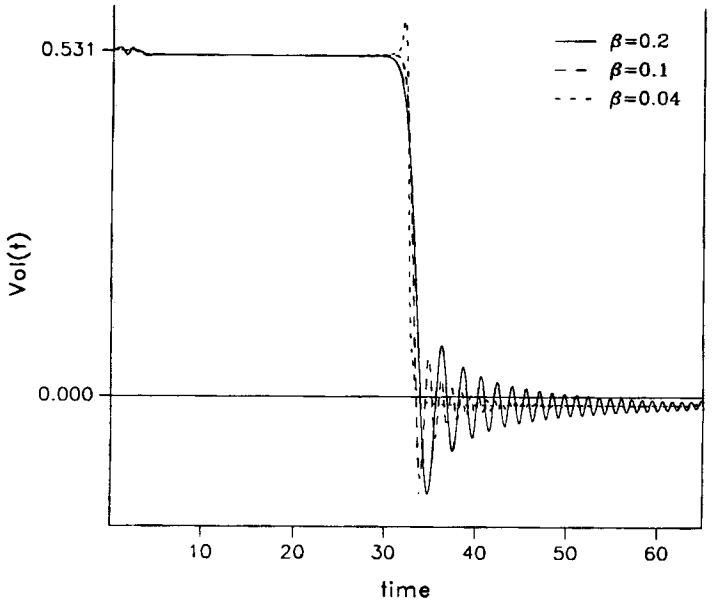

Figure 4. Volume excess Vol(t)

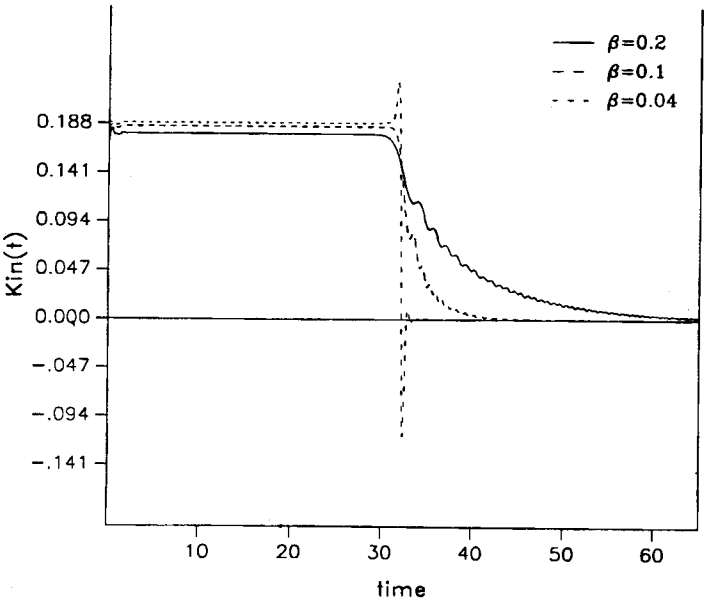

Figure 5. Kinetic energy Kin(t)

The constant C is the effective shallow water speed in the periodic medium. Thus long waves are delayed with respect to the flat bottom case, where $C=1$. Here $z=x/\sqrt{\varepsilon}$ is the fast variable. The function $h(z)$ is periodic with period unity and we get the auxiliary function $A(z, y)$ from the cell problem

$$A_{zz}+A_{yy}=0 \quad \text{in} \quad 0<z<1 \quad \text{and} \quad -h(z)<y<0, \tag{20}$$

with

$$A_y+h_zA_z=-h_z \quad \text{on} \quad y=-h(z),$$

$$A_y=0 \quad \text{on} \quad y=0.$$

We assume periodic dependence in z and we impose that the cell average $\iint_{\text{cell}} A(z, y)\,dz\,dy$ is zero.

We consider a simple case so that the problem above can be solved analytically and the numerical speed verified. Take a periodic bottom of the form

$$y=-h(z)=-[1-\sqrt{\varepsilon}\,n(z)].$$

We approximate the cell problem (20) by

$$A_{zz}+A_{yy}=0 \quad \text{in} \quad 0<z<1 \quad \text{and} \quad -1<y<0, \tag{21}$$

with

$$A_y+h_zA_z-\sqrt{\varepsilon}\,n(z)(A_{yy}+h_zA_{zy})+\frac{\varepsilon n^2(z)}{2}(A_{yyy}+h_zA_{zyy})+\cdots=-h_z \quad \text{at } y=-1,$$

$$A_y=0 \quad \text{at} \quad y=0.$$

We define for the bottom's profile

$$h(z)=1-\sqrt{\varepsilon}\sin(\pi z) \tag{22}$$

and we consider the expansion

$$A(z, y)=A^0(z, y)+\sqrt{\varepsilon}A^1(z, y)+\varepsilon A^2(z, y)+\varepsilon^{3/2}A^3(z, y)+\cdots,$$

with $\iint_{\text{cell}} A^j(z, y)\,dz\,dy=0$, $j=0, 1, \ldots$. We solve for each term in the expansion:

$$A^0(z, y)=A^2(z, y)=0, \qquad A^1(z, y)=\frac{-\cosh(\pi y)}{\sinh\pi}\cos(\pi z), \tag{23}$$

$$A^3(z, y)=-\frac{\pi^2}{8}\left(\frac{\cosh(\pi y)}{\sinh\pi}\cos(\pi z)-\frac{\cosh(3\pi y)}{2\sinh(3\pi)}\cos(3\pi z)\right). \tag{24}$$

The speed is computed approximately by using (23) and (24) in expression (19):

$$C^2=1-\varepsilon\frac{\pi}{\sinh\pi}\int_0^1\cosh[\pi h(z)]\cos^2(\pi z)\,dz-\varepsilon^2\frac{\pi^3}{8}\left(\frac{1}{\sinh\pi}\int_0^1\cosh[\pi h(z)]\cos^2(\pi z)\,dz\right.$$

$$\left.-\frac{1}{3\sinh(3\pi)}\int_0^1\cosh[3\pi h(z)]\cos(\pi z)\cos(3\pi z)\,dz\right)+\cdots. \tag{25}$$

We use a Gauss–Legendre quadrature for these integrals, with $h(z)$ given by (22). The resulting effective speed is $C=0{\cdot}993$ approximately when $\sqrt{\varepsilon}=0{\cdot}1$.

In our numerical experiment we approximate the sinusoidal bottom as a series of triangular bumps of base and height equal to $\sqrt{\varepsilon}$. We take the parameter β to be equal to $\sqrt{\varepsilon}$. We find the

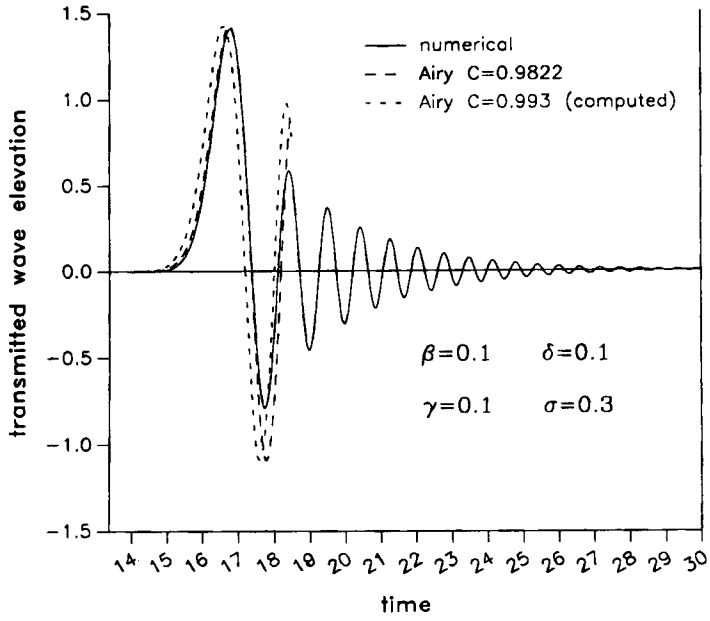

Figure 6. Slower effective speed due to periodic bottom

speed of the numerical solution by computing the Airy function as before, but with $x-Ct$ instead of $x-t$. The observed numerical speed is $C=0{\cdot}9822$. In Figure 6 we compare our results with the Airy function. Only the front of the Airy wave is shown. The numerical solution's speed and the effective shallow water speed disagree by only 1%. We discuss the discretization of the bottom at the end of the next subsection.

In Figure 6 we also show that the wavefront is exactly like the one for the flat bottom. We do not see any substantial reflection, which indicates that the bottom has been homogeneized (see also Figure 7). Making an analogy with composite materials, we can consider the rough periodic region as an effective homogeneous 'material' of smaller 'conductivity', since the effective speed is smaller. The theory we developed[1,8] can be used to show that in the presence of a rapidly varying periodic topography, no substantial reflection is generated.

3.3. Periodic versus random: numerical observation of localization

We now study the effect of a random component along the bottom's profile. We make a random perturbation (10% noise) of the periodic bottom described above. That is, we allow the heights of the triangles to be independent and uniformly distributed random variables in $[0{\cdot}09, 0{\cdot}11]$. We see in Figure 7 that randomness has a tremendous influence on the reflected signal observed at a fixed point to the left of the rough region. The bigger spike at the beginning is due to the transition from flat to rough. We have no reflection from the periodic bottom. The substantial change in the reflected signal, from such a small change in the bottom's profile, is a manifestation of localization. This means that all proper modes decay exponentially as they propagate in a random medium. The rate of decay depends on the wavelength and on the total length of the random region.[1,8,11,12]

We used linear boundary elements in the discretization of the bottom contour, one on each side of the triangular bumps. We conducted several tests to ensure that the coarse discretization and

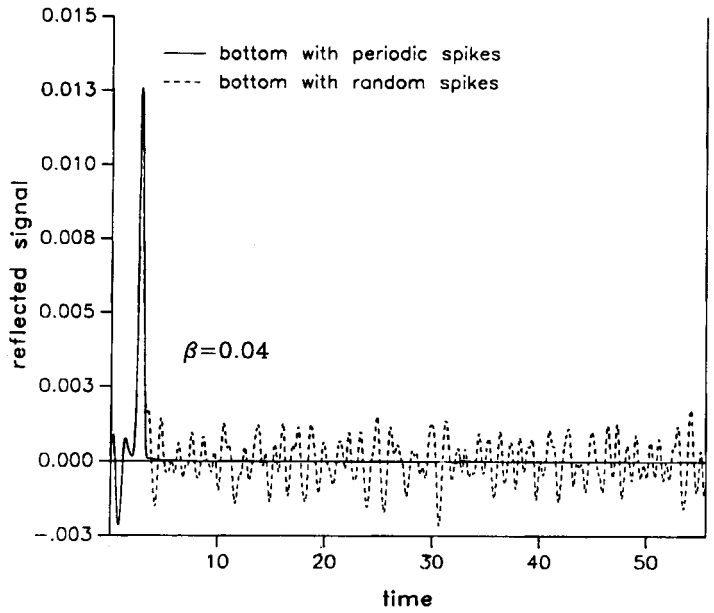

Figure 7. A periodic versus a random bottom

the sharp tips of each bump have no spurious effect on the reflected wave. We compared the two-element-per-bump discretization against a finer mesh with six elements per bump. The reflected signals are indistinguishable. We also considered six elements on a sinusoidal bump and compared them with the previous case. We found that no additional reflections are generated from the sharp tips of the bottom's irregularities.

We have developed an analytical theory for the statistics of the reflected wave.[1,8] We needed several realizations of the bottom's profile (by considering it as a stochastic process) in order to have a numerical verification of this theory. Thus an efficient and fast code was required. We concluded from the discretization study mentioned above that accuracy is maintained (regarding the reflected signal) when we use a coarse mesh along the bottom. Hence we were able to perform experiments in which the rough channels were long compared to the pulse-shaped wave. We present the comparison between the results from the asymptotic analysis of stochastic differential equations and the numerical experiments in Reference 1.

4. FINAL REMARKS

We studied numerically the linear water wave equations for shallow channels with a rapidly varying bottom topography. We used the boundary element method (BEM) to compute the propagation of surface waves for long times. The BEM gives an accurate approximation to the dispersion relation (by using $\theta=\frac{1}{6}$). We used linear elements which allow a straightforward vectorization of the code. Here is an example of the efficiency of the BEM. We discretized a long channel in which we had a mesh of 1044 nodes. The vectorized assemblage of the two non-symmetric dense matrices (for both the single- and double-layer potentials) is done in 1·4 s. A vectorized version of Linpack LU-factorizes ($O(N^3)$) the system's matrix in 5·4 s approximately and each time step takes 0·024 s. We used a total of 1800 time steps and a complete run takes

approximately 50·0 s of CPU time on an ETA10. For an even longer channel (used to generate Figure 3) we used a mesh with 2480 nodes and 4800 time steps. This experiment requires 13 Mwords of memory and takes approximately 7 min on a Cray Y-MP.

The experiments presented in this paper show that with the BEM we are able to capture several asymptotic properties of water waves. The long-time behaviour of a surface pulse-shaped wave is an important test regarding dispersive effects. The agreement with an Airy function shows that the dominant modes can be propagated accurately for large time intervals. We also showed that the code is robust in the shallow water regime for small but finite values of the parameter β. We saw the interaction between the surface wave and the rapidly varying periodic bottom through the effective shallow water speed. Finally we compared a periodic with a random topography. Even though the two channels were similar, the reflected waves generated were quite different.

We conclude that the BEM is a reliable method, with features that enabled the numerical reproduction of the results from the asymptotic theory for stochastic differential equations. The quantitative agreement between computation and theory is presented in Reference 1.

ACKNOWLEDGEMENTS

We are grateful to Dr. L. C. Wrobel for his useful comments regarding the boundary element method and to Professor Greg Baker for suggesting improvements to the paper. A. Nachbin's work has been supported by the Brazilian Ministry of Education and by The National Science Foundation under grant DMS 8701895 as was the work of G. Papanicolaou. The numerical calculations were done on an ETA10 at the John von Neumann National Supercomputer Center, Princeton, NJ. The experiment on the Cray Y-MP was done through resources provided by The Ohio Supercomputer Center, Columbus, OH.

APPENDIX: THE FINITE DIFFERENCE METHOD

In this appendix we comment briefly on numerical dispersion. We consider the channel to be flat and to have periodic boundary conditions at its right and left ends.

We discretize the free surface conditions as follows: for a point $x_j = j\Delta x$,

$$\frac{\phi^{n+1}-\phi^n}{\Delta t} = -\eta^{n+1} \qquad \text{(Bernoulli law at } t_{n+1}\text{)}, \tag{26}$$

$$\frac{D_p\phi^n}{\beta^2} = \frac{\eta^{n+1}-\eta^n}{\Delta t} \qquad \text{(kinematic condition at } t_n\text{)}, \tag{27}$$

where $D_p\phi$ is an approximation to $\phi_y(x_j, 0, t_n)$ using p nodes in the negative y-direction. We will study three different schemes for D_p.

We consider the Fourier mode

$$\phi(x_j, y_l, t_n) = \phi^n_{j,l} = Y(-l\Delta y)\exp[\mathrm{i}(kx_j - \omega t_n)] \tag{28}$$

in order to study the dispersive properties of the discretized problem. The function $Y(y)$ is unknown. We solve for $Y(y)$ by performing the discrete harmonic extension of a mode of amplitude $Y(0)$ given at the free surface. We eliminate η in (26), (27) and solve an $L \times L$ system of equations for the function $Y(-l\Delta y)$, $l = 1, \ldots, L$. We will show that the numerical dispersion relation is of the form

$$\frac{F_p(\Delta x, \Delta y; k, \beta)}{\beta^2} = 2\frac{1-\cos(\omega\,\Delta t)}{\Delta t^2}. \tag{29}$$

The numerical frequency is given by ω. It depends on the wave number k, the parameter β and the discretization adopted. A condition for stability (i.e. real-valued frequencies) is

$$\left|1-\frac{\Delta t^2}{2\beta^2}F_p\right|\leqslant 1. \tag{30}$$

Note that β small (shallow water) may require changes in the grid in order to avoid instabilities.

We now calculate the function F_p explicitly, where p indicates the number of nodes used for the discrete y-derivative. By Δ_j we denote the determinant of the submatrix obtained from the last j rows and columns of the linear system of equations. We substitute (28) in the standard (five-point molecule) difference scheme for the Laplacian to get

$$\begin{bmatrix} a & -1 & \cdots & 0 \\ -1 & a & \cdots & 0 \\ 0 & -1 & \cdots & 0 \\ \cdots & \cdots & \cdots & -1 \\ 0 & 0 & -1 & a-1 \end{bmatrix} \begin{bmatrix} Y_{-1} \\ Y_{-2} \\ \cdots \\ Y_{-L+1} \end{bmatrix} = \begin{bmatrix} Y_0 \\ 0 \\ \cdots \\ 0 \end{bmatrix}, \tag{31}$$

where

$$a=2+(\beta\bar{k}\Delta y)^2=2+r^2, \qquad L\Delta y=1 \quad \text{(uniform unit depth)}, \tag{32}$$

$$\bar{k}=\frac{\sqrt{\{2[1-\cos(k\Delta x)]\}}}{\Delta x}. \tag{33}$$

The coefficient Y_0 in the forcing term is due to the Dirichlet boundary condition at the top (i.e. a known value of the potential) and the coefficient $a-1$ is due to the Neumann condition along the impermeable flat bottom where the one-sided difference gives $Y_{-L+1}=Y_{-L}$.

By Cramer's rule $Y_{-1}=Y_0(\Delta_{L-2}/\Delta_{L-1})$, where these determinants satisfy the recurrence relation $\Delta_N=a\Delta_{N-1}-\Delta_{N-2}$. We consider solutions of the form λ^N which lead to the roots

$$\lambda_1=1+\frac{r^2}{2}+\frac{r}{2}\sqrt{(4+r^2)}, \qquad \lambda_2=1+\frac{r^2}{2}-\frac{r}{2}\sqrt{(4+r^2)}. \tag{34}$$

We get by straightforward manipulations that $\Delta_{L-2}/\Delta_{L-1}=\Lambda(\lambda_2)$, with

$$\Lambda(\lambda_2)=\lambda_2+\frac{1-\lambda_2^2}{\lambda_2}\frac{1}{1+\hat{\alpha}\lambda_2^{2-2L}}, \qquad \hat{\alpha}=\frac{\Delta_4-\lambda_2\Delta_3}{\Delta_3-\lambda_2\Delta_4}.$$

We now have a general formula for Y_{-1} only in terms of the root λ_2 and the total number of nodes in the y-direction ($L+1$—counting free surface and bottom), namely

$$Y_{-1}=Y_0\Lambda(\lambda_2). \tag{35}$$

By forward substitution we get

$$\begin{aligned} Y_{-2}&=Y_0[a\Lambda(\lambda_2)-1],\\ Y_{-3}&=Y_0[(a^2-1)\Lambda(\lambda_2)-a],\\ Y_{-4}&=Y_0[(a^3-2a)\Lambda(\lambda_2)-(a^2-1)]. \end{aligned}$$

We introduce the following approximate y-derivative formulae:

$$\text{two-point} \leftrightarrow D_2\,Y(y)=\frac{Y_0-Y_{-1}}{\Delta y} \quad \text{and} \quad F_2(\Delta x, \Delta y; k, \beta)=\frac{1}{\Delta y}[1-\Lambda(\lambda_2)], \tag{36}$$

$$\text{three-point} \leftrightarrow D_3\, Y(y) = \frac{3Y_0 - 4Y_{-1} + Y_{-2}}{2\Delta y} \quad \text{and} \quad F_3 = \left(1 - \frac{r^2}{2}\right) F_2 + \frac{r^2}{2\Delta y}, \tag{37}$$

$$\text{five-point} \leftrightarrow D_5\, Y(y) = \frac{25Y_0 - 48Y_{-1} + 36Y_{-2} - 16Y_{-3} + 3Y_{-4}}{12\Delta y} \quad \text{and}$$

$$F_5 = \frac{-(3a^3 - 16a^2 + 30a - 32)F_2}{12} + \frac{3a^3 - 19a^2 + 46a - 40}{12\Delta y}. \tag{38}$$

These are all one-sided difference schemes at the free surface $y=0$. We get the numerical dispersion relation corresponding to a given difference scheme by using these formulae in (29). The exact dispersion relation is

$$\omega^2 = \frac{k}{\beta}\tanh(k\beta). \tag{39}$$

We compare in Figures 8 and 9 different numerical dispersion curves against the exact one. We use a finer mesh in Figure 9 and obtain a better approximation to the exact dispersion curve. Convergence for the low frequencies is slower than for the higher ones.

We have decoupled the water wave equations in such a way that we solve two partial differential equations in succession: a boundary value problem at each time step and the evolution of its boundary data. We now verify that the numerical dispersion curve converges to the exact one. We start by computing the limiting value of the function F_p as $r \to 0$, keeping $L\Delta y = 1$. Note that $\lambda_2 \to 1$ and $\hat{\alpha} \to 1$ as $r \to 0$, that $\lambda_2^{-2L} \to e^{2k\beta}$ as $L \to \infty$ and therefore

$$\lim_{r\to 0}\left(\frac{1-\lambda_2^2}{r\lambda_2}\right)\frac{1}{1+\hat{\alpha}\lambda_2^{9-2L}} = \frac{2}{1+e^{2k\beta}}.$$

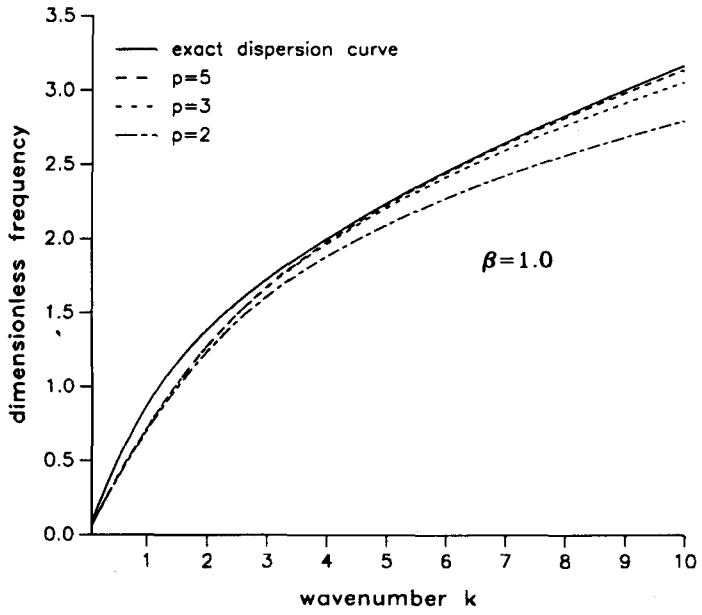

Figure 8. Dispersion curves for different approximations of $\phi_y(x, 0, t)$. The spacing is $\Delta x = 1/40$, $\Delta y = 1/20$ and $\Delta t = 1/40$

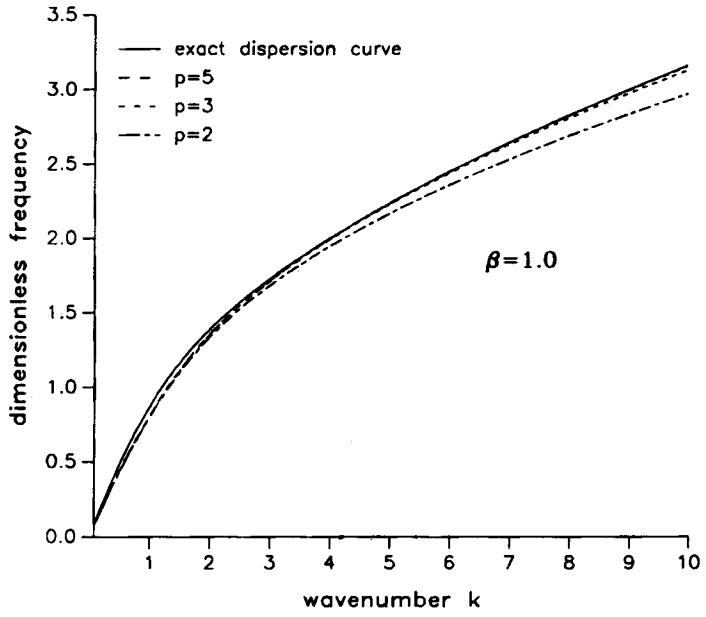

Figure 9. Dispersion curves for different approximations of $\phi_y(x, 0, t)$. The spacing is $\Delta x = 1/80$, $\Delta y = 1/40$ and $\Delta t = 1/80$

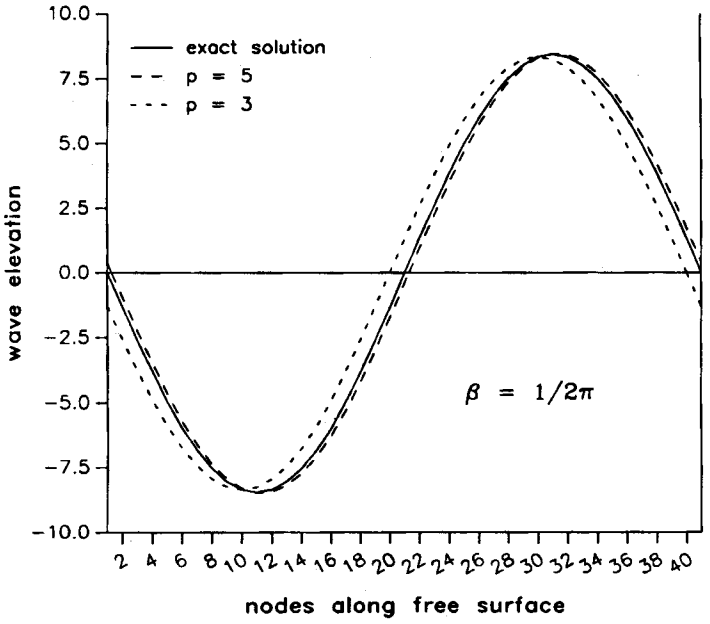

Figure 10. Results when the approximation of $\phi_y(x, 0, t)$ is improved. The node spacing used is $\Delta x = 2\pi/40$, $\Delta y = 1/20$ and $\Delta t = 114{\cdot}5877/4000$

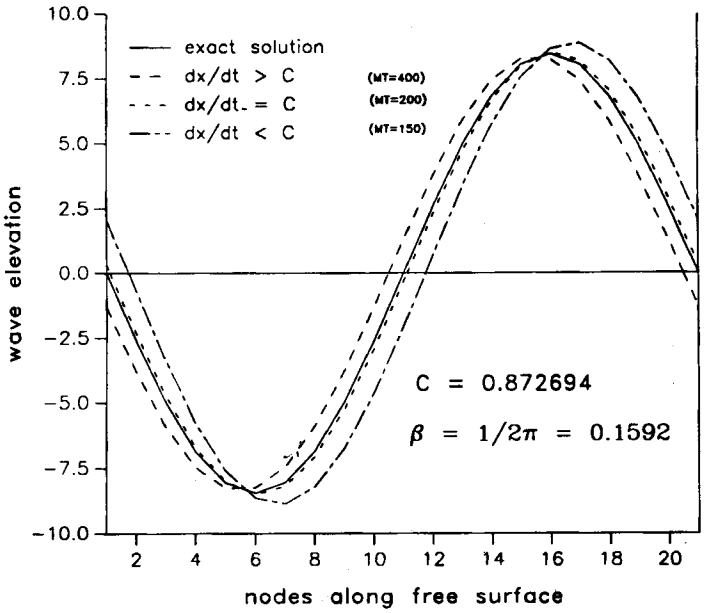

Figure 11. Results showing the $\Delta x/\Delta t$ dependence. The node spacing is $\Delta x = 2\pi/20$, $\Delta y = 1/10$ and $\Delta t = 11{\cdot}45877/MT$

We use this result in connection with each function F_p and we let Δx and Δt go to zero. The limiting form of the numerical dispersion relation (29) follows. It agrees with the exact dispersion relation for each value of p ($p=2, 3, 5$). The order in which we let Δx, Δy and Δt go to zero does not affect the convergence but is important for stability. If we violate the stability condition, $\omega \to \omega_{\text{exact}}$ through the complex plane.

We have introduced an error which is second-order in the mesh size (by solving the discrete Laplacian). We used these approximate values of ϕ to calculate the discrete y-derivative $D_p\phi$ ($p=2, 3, 5$). The interesting fact is that higher-order schemes (such as $p=3$ and 5) will lead to a more accurate numerical dispersion relation even though we started with a second-order approximation of ϕ (see Figures 8 and 9). We observed this numerically and the results are presented in Figure 10.

The essence of the discussion above is that the discrete y-derivative must be computed accurately. We immediately see an advantage of the BEM with respect to the FDM: no discrete y-differencing is needed. The quantity ϕ_y is obtained directly from the system of equations.

Finally we also observed numerically that the evolution of η depends on the ratio $\Delta x/\Delta t$. The optimal ratio is $\Delta x/\Delta t = C(k)$, the phase speed, which is very restrictive when we superimpose different modes. Figure 11 shows how this ratio affects the propagation of a single mode.

REFERENCES

1. A. Nachbin and G. C. Papanicolaou, 'Water waves in shallow channels of rapidly varying depth', accepted for publication in the *J. Fluid. Mech.*
2. J. Hamilton, 'Differential equations for long-period gravity waves on a fluid of rapidly varying depth', *J. Fluid Mech.*, **83**, 289–310 (1977).
3. G. B. Whitham, *Linear and Nonlinear Waves*, Wiley, New York, 1974.
4. R. R. Rosales and G. C. Papanicolaou, 'Gravity waves in a channel with a rough bottom', *Stud. Appl. Math.*, **68**, 89–102 (1983).

5. J. R. Salmon, P. L.-F. Liu and J. A. Liggett, 'Integral equation method for linear water waves', *J. Hydraul. Div., ASCE*, **106**, 1995–2010 (1980).
6. C. A. Brebbia, J. C. F. Telles and L. C. Wrobel, *Boundary Element Technique*, Springer, New York, 1984.
7. T. Nakayama and K. Washizu, 'The boundary element method applied to the analysis of two-dimensional nonlinear sloshing problems', *Int. j. numer. methods eng.*, **17**, 1631–1646 (1981).
8. A. Nachbin, 'Reflection and transmission of water waves in shallow channels with rough bottoms', *Ph.D. Thesis*, Courant Institute, New York University, 1989.
9. W. H. Press, B. P. Flannery, S. A. Teukolsky and W. T. Vetterling, *Numerical Recipes, The Art of Scientific Computing*, Cambridge University Press, Cambridge, 1987.
10. J. J. Stoker, *Water Waves*, Interscience, New York, 1957.
11. P. Devillard, F. Dunlop and B. Souillard, 'Localization of gravity waves on a channel with a random bottom', *J. Fluid Mech.*, **186**, 521–538 (1988).
12. G. C. Papanicolaou, 'Asymptotic analysis of stochastic equations', in M. Rosenblatt (ed.), *MAA Studies in Mathematics, Vol. 18, Studies in Probability*, The Mathematical Association of America, 1978, pp. 111–179.